Numerical Modelling of Train Induced Vibrations

Riccardo Ferrara, Giovanni Leonardi, Franck Jourdan

Numerical Modelling of Train Induced Vibrations

Authors:
Ferrara R.
PhD Student – University of Reggio Calabria, University Montpellier 2 – riccardo.ferrara@unirc.it

Leonardi G.
Associate Professor – University of Reggio Calabria – giovanni.leonardi@unirc.it

Jourdan F.
Professor – University Montpellier 2 – franck.jourdan@univ-montp2.fr

ABSTRACT

In this paper a numerical model to predict train induced vibration is presented. The dynamic computation considers mutual interactions in vehicle/track coupled systems by means of a finite and discrete elements method. The considered vehicle model consists of 7 two-dimensional discrete elements connected by spring/damper couples. The rail is modeled as finites beam elements connected to sleepers by pads areas. Supporting substructure consisting of pads, sleepers, ballast and foundation, is modelled as discrete elements. Components are connected each to others by spring/damper couples. Vertical profile of rail is considered as sum of trigonometric functions with phase and amplitude generated by a pseudo random process. The dynamic interaction between the wheel-sets and the rail is accomplished by using the non-linear Hertzian theory.

The strong point of this study consists in the model used to simulate the behaviour of pads. The rail-sleeper contact is assumed extended to an area defined such a contact-zone, rather than a single point assumption which fits better real case studies. Experimental validations show how prediction fits well experimental data.

Keywords: train, railway, vibrations, sleeper, wheel-rail, contact force.

INTRODUCTION

Modelling and predicting vibrations is not an immediate process due to the several parameters, the heterogeneity of track properties and corrugation, the behaviours of materials. For this fact, to have a good prediction of vibrations, it is necessary to focus the precision of model on the phenomenons with more impact. The main causes of vibrations induced by train are: rail irregularity, wheel defects and variation of stiffness due to discrete supporting of rail. The first two phenomenons have been abundantly discussed by numerous works. They are diversified by the models employed for the vehicle and the track. Some works [4, 8, 15] have studied the waves propagation through the track-ground system in three dimensions, modelling contact forces as constant or harmonic vertical forces moving along the rails. Others [11, 12, 14] have studied the coupled train/track system in two dimensions, modelling rail as a Timoshenko beam connected to pads by singular point. Still others [9, 10] have studied the coupled system modelling rail with finite elements connected to pads by singular points; they have discretized the rail with a singular finite element for each pair of sleepers. However the rail is connected to sleepers by a contact zone not negligible if compared to the length of the rail suspended between two consecutive sleepers. Indeed, sleeper base measures between 60 and 70 cm and the pad length along the rail direction measures between 17 and 26 cm. In addition the midspan point of rail assumes the maximum displacement during vibration and this cannot be modelled with a singular element between two sleepers. Moreover shear effects for rail finite elements are neglected in [9, 10], but the height of rail section (148 mm for a 50 UNI rail and 172 mm for a 60 UIC rail [13]), compared to length of a beam element, is not small enough to allow classical hypothesis for slender beams.

In this work we have treated all of three phenomenons: rail irregularity, wheel defects and variation of stiffness due to discrete supporting of rail. The main difference from present work and the others consists in the model of connection between rail and sleepers. A contact-zone has been considered. A series of spring/damper elements have been placed along all the longitudinal length of the sleepers. The number of elements can be chosen in the algorithm.

1. DESCRIPTION OF THE MODEL

The vehicle is modelled as 7 two-dimensional rigid elements representing: the body, the two boogies and the four wheels. The total number of degrees of freedom considered for the vehicle is 10: the vertical displacement for all of seven rigid elements, the pitch of body and wheels.

Railway is discretized as finite Timoshenko beam elements. For each beam element, 4 degrees of freedom are considered: vertical displacement and rotation of every node. Axial deformation is insignificant.

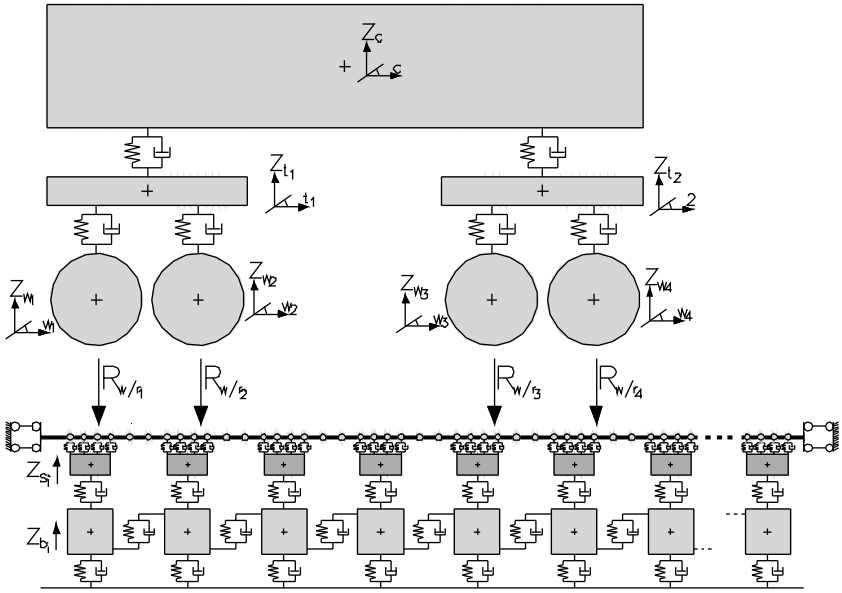

Figure 1: Draft of the model.

The substructure is made-up of: rail-pads, sleepers, ballast, and background. Comparing mass and stiffness between rail-pads and concrete sleepers it results that rail-pads mass (1∼2 kg) is negligible with respect to concrete sleepers mass (250∼350 kg). Similarly, sleeper vertical stiffness ($30\sim40\cdot10^{12}$ N m^{-1}) is six orders of magnitude bigger than pad vertical stiffness ($15\sim25\cdot10^{6}$ N m^{-1}). For this fact, rail-pads have been modelled as spring/damper couples without mass and sleepers have been modelled as rigid elements. Moreover many spring/damper couples are disposed along the length of sleepers to better fit the contact area. The vertical stiffness and the mass of the ballast are both significant, so the ballast has been modelled as blocks made-up of rigid elements, connected to sleeper by spring/damper couples. To allow the transmission of vibrations in longitudinal direction too, spring/damper couples connect ballast elements horizontally. Ballast stiffness is calculated according to Zhai et al. [17], so the stiffness for a ballast block is:

$$k_b = \frac{2(l_s - b_s)\tan\phi}{\ln\left[\dfrac{l_s(2h_b\tan\phi + b_s)}{b_s(2h_b\tan\phi + l_s)}\right]} E_b \,, \tag{1}$$

where:

ϕ : internal friction angle of ballast;

l_s, b_s : dimensions of the effective contact area between ballast and sleepers;

h_b : height of ballast;

E_b : modulus of elasticity of ballast.

In accordance with Y.Q. Sun and Dhanasekar [14] coefficients for longitudinal springs and dampers are calculated as 30% of respective vertical coefficient.

To represent the behaviour of background a spring/damper couple is added over ballast blocks (see Figure 1).

2. ASSEMBLING MOTION EQUATIONS

The motion equations associated to the vehicle degrees of freedom have been written in accordance with X. Lei and Noda [9] in the matrix form:

$$\boldsymbol{M}_v \ddot{\boldsymbol{z}}_v + \boldsymbol{C}_v \dot{\boldsymbol{z}}_v + \boldsymbol{K}_v \boldsymbol{z}_v = \boldsymbol{r}_{r/w}(z_v, z_r) - \boldsymbol{p}_v \,, \tag{2}$$

where:

$\boldsymbol{M}_v, \boldsymbol{C}_v, \boldsymbol{K}_v$: mass, stiffness and damping matrices;

$\ddot{\boldsymbol{z}}_v, \dot{\boldsymbol{z}}_v, \boldsymbol{z}_v$: accelerations, speeds, displacements vectors;

$\boldsymbol{p}_v, \boldsymbol{r}_{r/w}$: weight forces and wheel-rail contact forces vectors.

The contact force for the j^{th}-wheel has been computed by the non-linear Hertz model as:

$$R_{r/w,j} = \begin{cases} k_h \delta^{1,5} + c_h \dot{\delta} & if \;\; \delta > 0 \\ 0 & if \;\; \delta < 0 \end{cases}, \tag{3}$$

where:

k_h : Hertzian contact coefficient computed by Y.Q. Sun et Al. [14];

c_h : represents the combination of two physical phenomenons: the friction and the viscosity of material;

δ : total deformation of wheel and rail.

The total deformation of wheel and rail is computed as:

$$\delta = z_{wj} - z_{rj} - \eta_{rj} \,, \tag{4}$$

where:

z_{wj} : the vertical displacement of the j^{th}-wheel;

z_{rj}, η_{rj} : displacement and vertical defect of rail at j^{th}-contact-point respectively.

Vertical defect has been computed in accordance with Lei and N.A. Noda [9].
Similar to Equation (2), the dynamic equation associated to rail nodes can be written in the matrix form:

$$\boldsymbol{M}_r \ddot{\boldsymbol{z}}_r + \boldsymbol{C}_r \dot{\boldsymbol{z}}_r + \boldsymbol{K}_r \boldsymbol{z}_r = -\boldsymbol{r}_{w/r}(z_v, z_r) - \boldsymbol{r}_{s/r}(z_r, z_s) - \boldsymbol{p}_r \,, \tag{5}$$

where:

$\boldsymbol{p}_r$: equivalent nodal loads vector containing the weight forces;

$\boldsymbol{r}_{w/r}$: equivalent nodal loads vector containing the wheel-rail contact forces;

$\boldsymbol{r}_{s/r}$: nodal loads vector containing the sleeper-rail contact forces.

Damping matrix has been calculated by Raylegh's theory as linear function of mass and stiffness matrices.
Similar to Equations (2) and (4), the dynamic equation associated to substructure can be written in the matrix form:

$$\boldsymbol{M}_s \ddot{\boldsymbol{z}}_s + \boldsymbol{C}_s \dot{\boldsymbol{z}}_s + \boldsymbol{K}_s \boldsymbol{z}_s = -\boldsymbol{r}_{r/s}(z_r, z_s) - \boldsymbol{p}_s \,, \tag{6}$$

where:

$\boldsymbol{p}_s$: weight forces;

$\boldsymbol{r}_{r/s}$: rails-sleeper contact forces.

Finally it's possible to assemble the systems of equations (2), (5) and (6), in one system:

$$\boldsymbol{M}\,\ddot{\boldsymbol{z}}+\boldsymbol{C}\,\dot{\boldsymbol{z}}+\boldsymbol{K}\,\boldsymbol{z}=-\boldsymbol{r}\left(z_v,\,z_r,\,z_s\right)-\boldsymbol{p}\ . \tag{7}$$

3. RESOLUTION OF MOTION EQUATIONS

In order to solve the non linear system of equation (7), displacements and speeds have been written as function of accelerations by the linear acceleration method. Then we have:

$$\boldsymbol{F}\left(\ddot{\boldsymbol{z}}_{i+1}\right)=\boldsymbol{A}\,\ddot{\boldsymbol{z}}_{i+1}+\boldsymbol{f}_{i+1}\left(\ddot{\boldsymbol{z}}_{i+1}\right)-\boldsymbol{b}_i=\boldsymbol{0}\ , \tag{8}$$

where:

$$\boldsymbol{A}=\boldsymbol{M}+\frac{\Delta t}{2}\boldsymbol{C}+\frac{\Delta t^2}{6}\boldsymbol{K}\ , \tag{9}$$

$$\boldsymbol{b}_i=-\boldsymbol{p}-\boldsymbol{C}\left(\dot{\boldsymbol{z}}_i+\frac{\Delta t}{2}\ddot{\boldsymbol{z}}_i\right)-\boldsymbol{K}\left(\boldsymbol{z}_i+\Delta t\,\dot{\boldsymbol{z}}_i+\frac{\Delta t^2}{3}\ddot{\boldsymbol{z}}_i\right), \tag{10}$$

$$\ddot{\boldsymbol{z}}_{i+1}=\begin{bmatrix}\ddot{\boldsymbol{z}}_{v,\,i+1}\\ \ddot{\boldsymbol{z}}_{r,\,i+1}\\ \ddot{\boldsymbol{z}}_{s,\,i+1}\end{bmatrix}, \tag{11}$$

$$\boldsymbol{f}_{i+1}=\begin{bmatrix}-\boldsymbol{r}_{r/w}\left(z_v,\,z_r\right)\\ \boldsymbol{r}_{w/r}\left(z_v,\,z_r\right)+\boldsymbol{r}_{s/r}\left(z_r,\,z_s\right)\\ \boldsymbol{r}_{r/s}\left(z_r,\,z_s\right)\end{bmatrix}. \tag{12}$$

The variables at the i^{th} time step are knowns. The number of equations is $n_{eq}=10+2\,n+2\,m$, where 10 is the number of degrees of freedom of the vehicle, n is the number of rail nodes, and m is the number of sleepers included in the route considered.

This system of equations has been solved with the Raphson iterative method. The Jacobian associated to system of equation (8) is:

$$\boldsymbol{J}\left(\ddot{\boldsymbol{z}}_{i+1}^{k}\right)=\boldsymbol{A}+\begin{bmatrix}\boldsymbol{0}_{6\times 6} & \boldsymbol{0}_{6\times(4+2\mathrm{n})} & \boldsymbol{0}_{6\times 2\mathrm{m}}\\ \boldsymbol{0}_{(4+2\mathrm{n})\times 6} & \boldsymbol{R}\left(\ddot{\boldsymbol{z}}_{i+1}^{k}\right)_{(4+2\mathrm{n})\times(4+2\mathrm{n})} & \boldsymbol{0}_{(4+2\mathrm{n})\times 2\mathrm{m}}\\ \boldsymbol{0}_{2\mathrm{m}\times 6} & \boldsymbol{0}_{2\mathrm{m}\times(4+2\mathrm{n})} & \boldsymbol{0}_{2\mathrm{m}\times 2\mathrm{m}}\end{bmatrix}, \tag{14}$$

where $\boldsymbol{R}\left(\ddot{\boldsymbol{z}}_{i+1}^{k}\right)_{(4+2\mathrm{n})\times(4+2\mathrm{n})}$ is a matrix which contains the derivatives of the components of the vector $\boldsymbol{f}_{i+1}$ with respect to accelerations. The component at the line l and at the column c is:

$$R_{l,\,c}=\frac{\partial f_l}{\partial\,\ddot{z}_c}\ . \tag{15}$$

Once the Jacobian is defined, the solution $\ddot{\boldsymbol{z}}_{i+1}$ can be calculated as limit of the sequence $\left[\ddot{\boldsymbol{z}}_{i+1}^{k}\right]_{k\,\in\,\mathbb{N}}$ where the superscript k is relative to the k^{th} $R.$ iteration, such that:

$$\boldsymbol{J}\left(\ddot{\boldsymbol{z}}_{i+1}^{k}\right)\left(\ddot{\boldsymbol{z}}_{i+1}^{k+1}-\ddot{\boldsymbol{z}}_{i+1}^{k}\right)=-\boldsymbol{F}\left(\ddot{\boldsymbol{z}}_{i+1}^{k}\right)\ . \tag{16}$$

4. COMPARISON WITH OTHER NUMERICAL MODELS

A comparison with other models has been done to validate the present work. Two cases are considered: a rail with simple corrugation and one with an irregularity based on ISO3095 [1] limit curve.

First the case of a corrugated rail with regular defects is considered. In Figure 2 a comparison between our numerical results and those of J. Zhang et al. [19] is shown. The parameters for the vehicle are taken from [19]. The track consists of 100 sleepers, the rail between two consecutive sleepers is divided in 12 beam elements, vehicle speed is 160 km/h. Track parameters are reported in Table 1. The wavelength and the depth of defects are 3,3 cm and 25 μm respectively. The trend of wheel-rail contact force is shown in Figure 2(a). In Figure 2(b) the rail deformation for a given time step is shown. The value of the subgrade equivalent stiffness is infinity (biggest number supported by MATLAB), because this level of elasticity has not been considered by J. Zhang et al. [19].

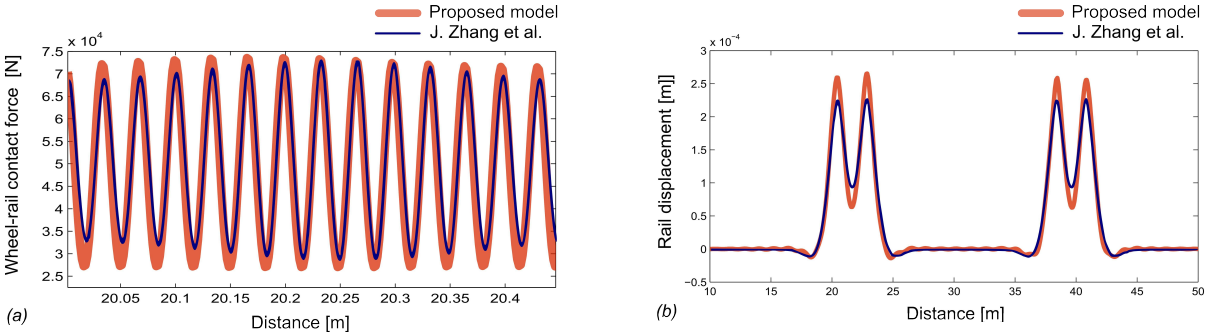

Figure 2: Comparison between J. Zhang et al [19] and presented model in case of regular corrugation: (a) wheel-rail contact force and (b) rail displacement.

It results that both of the curves fit well with other model. Focusing on Figure 2(a) it's possible to see how both of curves appear like modulated carrier waves. The carrier frequency, 1347 Hz, corresponds to the wavelength of corrugation: 3,3 cm. It causes the biggest variation of the dynamic contact force. The lower and upper sideband frequencies are 1347 ± 81.5 Hz, where 81.5 Hz corresponds to the sleeper passing frequency. The Fourier spectrum of contact force is shown in Figure 3.

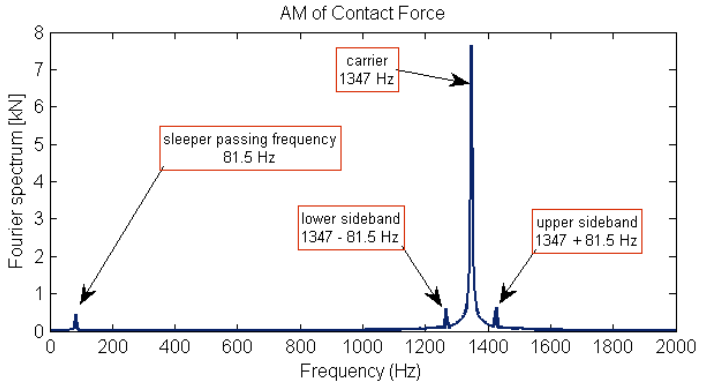

Figure 3: Amplitude modulation of contact force in proposed model.

Looking on Figure 2(a) It's possible to see how the modulation index is bigger in the J. Zhang et al. [19] model than the proposed one. This could be explained by the difference between the sleeper-rail contact-zone introduced in this paper and the singular point contact model. In fact the stiffness of the track, encountered by the rolling wheel, varies faster near a singular contact point, and the contact-force has to variate with the same trend. On the contrary in the contact area model this variation has to be less conspicuous because the stiffness is not concentrated on a point.

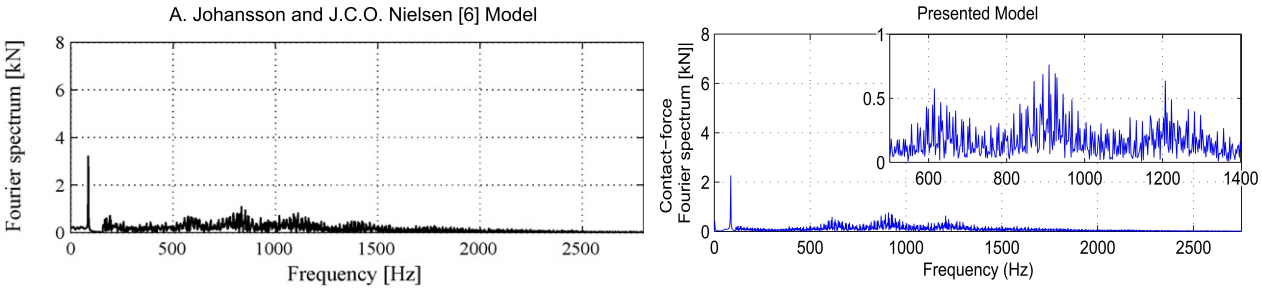

(a) (b)

Figure 4: Comparison between A. Johansson and J.C.O. Nielsen [7] model and the proposed one in case of ISO3095 [1] based corrugation:
(a) Fourier spectrum of the normal contact force for Johansson & Nielsen [7]; (b) Fourier spectrum of the normal contact-force calculated with present model.

In the second case a rail with corrugation based on ISO3095 [1] is considered. The modal frequency analysis of the contact-force has been compared with the A. Johansson and J.C.O. Nielsen [7] model. The parameters of the model are reported in Table 2.

The comparison between models is shown in Figure 4. The biggest amplitude of the normal contact-force Fourier spectrum corresponds to the sleeper passing frequency: 85 Hz. Focusing on Figure 4(b), amplitudes increase in magnitude around 570 Hz, 830 Hz, 1100 Hz and 1420 Hz. These frequencies correspond to the bending modes of a rail, with pinned-pinned boundary conditions, considering the same length of the boogie wheelbase [6, 16]. Experimental results confirm this behaviour [7].

Table 1: Model parameters adopted in the 1st case.

notation	parameter	value	unit
	Model parameters of substructure		
E	Young modulus of rail	$2{,}07 \cdot 10^{11}$	N m^{-1}
I	inertial modulus of rail	$3217 \cdot 10^{-8}$	m^4
A	section area of rail	$76{,}2 \cdot 10^{-4}$	m^2
χ	Timoshenko shear coefficient	0,34	
m_r	railway mass (per unit length)	60,64	kg m^{-1}
M_s	sleepers mass	125	kg
k_p	pad stiffness	$10 \cdot 10^{7}$	N m^{-1}
c_p	pad damping	$20 \cdot 10^{3}$	N s m^{-1}
k_b	ballast stiffness	$30 \cdot 10^{7}$	N m^{-1}
c_b	ballast damping	$58{,}8 \cdot 10^{3}$	N s m^{-1}
l_s	sleeper base	54,5	cm
	Other simulation parameters		
dt	time step	$1{,}8 \cdot 10^{-5}$	s
K_h	Hertz contact coefficient	$0{,}87 \cdot 10^{11}$	N m$^{-3/2}$
L_s	simulation line length	65	m
n	number of pad elements	6	
d	number of beams between sleepers	6	

Table 2: Model parameters adopted in the 2nd case.

notation	parameter	value	unit
	Model parameters of substructure[a]		
E	Young modulus of rail	$2{,}07 \cdot 10^{11}$	N m^{-1}
I	inertial modulus of rail	$3096 \cdot 10^{-8}$	m^4
A	section area of rail	$77{,}00 \cdot 10^{-4}$	m^2
c	Timoshenko shear coefficient	0,34	
m_r	railway mass (per unit length)	60	kg m^{-1}
M_s	sleepers mass	125	kg
k_p	pad stiffness	$120 \cdot 10^{6}$	N m^{-1}
c_p	pad damping	$16 \cdot 10^{3}$	N s m^{-1}
k_b	ballast stiffness	$140 \cdot 10^{6}$	N m^{-1}
c_b	ballast damping	$165 \cdot 10^{3}$	N s m^{-1}
l_s	sleeper base	65	cm
	Model parameters of train *x2000*		
$2M_c$	car body mass	28900	kg
M_b	bogie mass	1630	kg
$2M_w$	wheelset mass	2000	kg
$2l_b$	wheelset base	4,1	m
$2l_w$	bogie base	17,7	m
k_1	primary suspension stiffness	328	kN m^{-1}
k_2	secondary suspension stiffness	131	kN m^{-1}
c_1	primary suspension damping	30	kN s m^{-1}
c_2	secondary suspension damping	90	kN s m^{-1}
	Other simulation parameters		
dt	time step	$5{,}9 \cdot 10^{-5}$	s
K_h	Hertz contact coefficient	$0{,}87 \cdot 10^{11}$	N m$^{-3/2}$
C_h	contact damping coefficient	$1{,}5 \cdot 10^{5}$	N s m^{-1}
L_s	simulation line length	64,45	m
n	number of pad elements	30	
d	number of beams between sleepers	12	
N	number of defects functions	500	
ω_u	upper pulsation	2778	rad s^{-1}
ω_l	lower pulsation	112	rad s^{-1}
V	train velocity	200	km h^{-1}

a: parameters taken from [6]

5. VALIDATION WITH EXPERIMENTAL RESULTS

A real case has been studied to validate the efficiency of the model. The railway section, 64.35 m long, is relative to the Italian line Alcamo-Marsala (116 km). It's an old line with wooden sleepers. G. Di Mino et al. [3] have carried out measurements in this railway line with a series of accelerometers. They considered a running of an *ALn668* train with single configuration, having velocity of 90 km h^{-1}. A comparison between experimental and numerical results of the rail vertical accelerations is presented in Figure 5. Similarly, the sleeper vertical accelerations are reported in Figure 6. All of parameters adopted in the model are reported in Table 3.

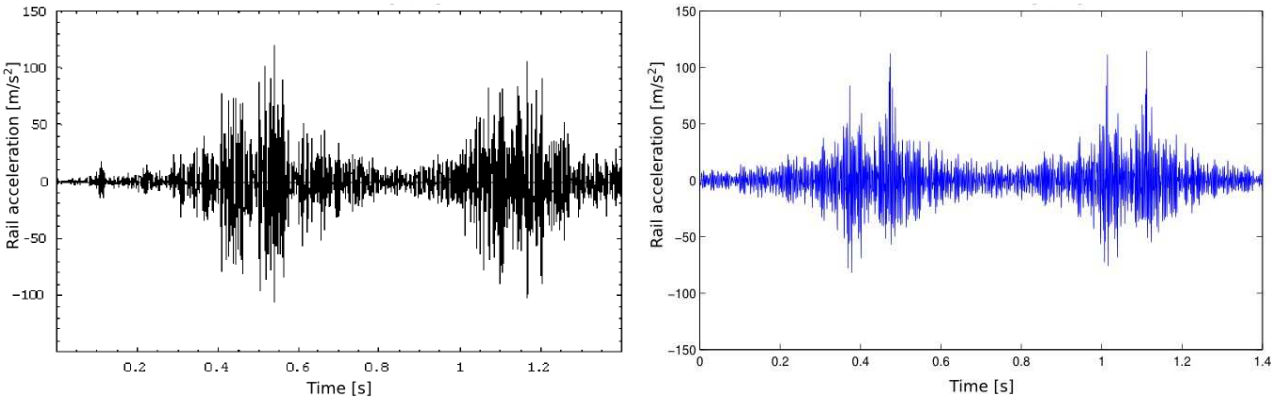

Figure 5: Comparison between: (a) experimental data [3] and (b) numerical results of the rail vertical acceleration in the first case.

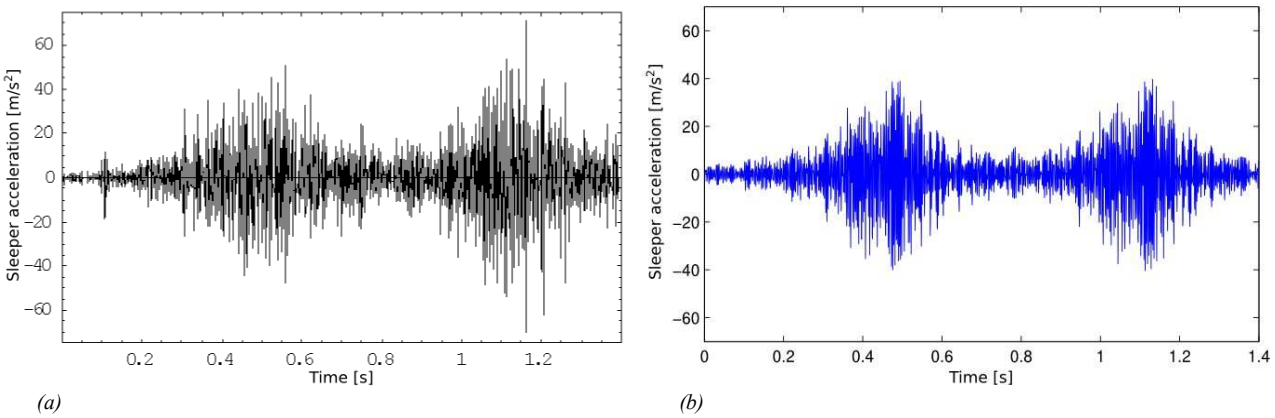

Figure 6: Comparison between: (a) experimental data [3] and (b) numerical results of the sleeper vertical acceleration in the first case.

Experimental data in Figure 5(a) shows that peaks of the rail vertical acceleration are included between 50 ms^{-2} and 100 ms^{-2}, and they occur in correspondence of the four wheels-sets passage. The same behaviour is predicted by numerical simulation in Figure 5(b). In Figure 6(a) the peaks are not distinguishable for each wheel-set. Figure 6(b) shows that our model well predict also this kind of behaviour.

Table 3: Model parameters adopted for the simulation

notation	parameter	value	unit
	Model parameters of substructure[a]		
E	Young modulus of rail	$2{,}07 \cdot 10^{11}$	N m^{-1}
I	inertial modulus of rail	$1884 \cdot 10^{-8}$	m^4
A	section area of rail	$63{,}62 \cdot 10^{-4}$	m^2
c	Timoshenko shear coefficient	0,34	
m_r	railway mass (per unit length)	49,9	kg m^{-1}
M_s	sleepers mass	33	kg
M_b	ballast mass	700	kg
k_p	pad stiffness	$26{,}5 \cdot 10^{7}$	N m^{-1}
c_p	pad damping	$40 \cdot 10^{3}$	N s m^{-1}
k_b	ballast stiffness	$24 \cdot 10^{7}$	N m^{-1}
c_b	ballast damping	$58{,}8 \cdot 10^{3}$	N s m^{-1}
k_w	horizontal stiffness	$7{,}84 \cdot 10^{7}$	N m^{-1}
c_w	horizontal damping	$80 \cdot 10^{3}$	N s m^{-1}
k_f	subgrade stiffness	$7{,}68 \cdot 10^{7}$	N m^{-1}
c_f	subgrade damping	$64{,}6 \cdot 10^{3}$	N s m^{-1}
l_s	sleeper base	65	cm
	Model parameters of train *Aln668*[a]		
$2M_c$	car body mass	28800	kg
M_b	bogie mass	3600	kg
$2M_w$	wheelset mass	500	kg
l_c	total length	23540	mm
$2l_b$	wheelset base	2,45	m
$2l_w$	bogie base	15,95	m
k_1	primary suspension stiffness	500	kN m^{-1}
k_2	secondary suspension stiffness	8800	kN m^{-1}
c_1	primary suspension damping	0,5	kN s m^{-1}
c_2	secondary suspension damping	41,5	kN s m^{-1}
	Other simulation parameters		
dt	time step	$6 \cdot 10^{-5}$	s
K_h	Hertz contact coefficient	$0{,}87 \cdot 10^{11}$	N m$^{-3/2}$
C_h	contact damping coefficient	$3 \cdot 10^{5}$	N s m^{-1}
L_s	simulation line length	64,45	m
n	number of pad elements	7	
d	number of beams between sleepers	9	
N	number of defects functions	200	
ω_u	upper pulsation	1560	rad s^{-1}
ω_l	lower pulsation	12	rad s^{-1}
I_{lg}	line grade index	1	
V	train velocity	90	km h^{-1}

a: parameters taken from [2]

6. CONCLUSIONS

The model presented in this work allows to predict contact forces and vibrations in all of vehicle and track components. The validation shows how prediction fits well experimental data and numerical data of other models.

Studying the Fourier spectrum of contact-force in the case of regular defects it has seen that the contact-force can be treated as an amplitude modulated wave. The carrier frequency is $f = V/\lambda$, where V is the train speed and λ is the wavelength of defect; the upper and lower sidebands can be calculated adding and subtracting the sleeper passing frequency from the carrier signal. It has noticed that singular point models overestimate modulation index.

The model of rail support, here introduced, can be more accurate especially for modal analysis of contact-force and vibrations. In future works we will study new scenarios working on modal analysis.

REFERENCES

[1] Bracciali, A. (2004). "Long roughness measurements – Analysis and possible protocol". *Proceeding of 8th International Workshop on Railway Noise,* Buxton, UK, ISBN:9788890437007, 0-0.

[2] Cantone, L., Negretti, D., Vita, L. and Vullo, V. (2009). "Effect of train longitudinal dynamics on wheel-rail forces". *Proceeding of 8th International Conference on Contact Mechanics and Wear of Rail/Wheel Systems*, Firenze, Italy.

[3] Di Mino, G., Di Liberto, C. and Nigrelli, J. (2007). "A FEM model of rail track-ground system to calculate the ground borne vibrations: a case of rail track with wooden sleepers and k-fastenings at Castelvetrano". *Proceeding of Advanced Characterisation of Pavement and Soil Engineering Materials*, Athens, Greece.

[4] Ekevid, T., Li, M.X.D. and Wiberg, N.E. (2001). "Adaptive FEA of wave propagation induced by high-speed trains". *Computers and Structures,* 79, 2693-2704.

[5] Fermér, M. and Nielsen, J.C.O. (1995). "Vertical interaction between train and track with soft and stiff rail pads – full-scale experiments and theory". *Proceeding of the Institution of Mechanical Engineers*, 209, 39-47.

[6] Igeland, A. (1996). "Rail corrugation growth ex5plained by interaction between track and bogie wheelsets". *Proceeding of the Institution of Mechanical Engineers*, part F 210 (1), 11-20.

[7] Johansson, A., Nielsen, J.C.O. (2007). "Rail roughness growth - influence of powered wheelsets with wheel tread irregularities". *Wear,* 262, 1296–1307.

[8] Karlström, A ., (2006), " An analytical model for ground vibrations from accelerating trains". *Journal of Sound and Vibration ,* 293, 587-598.

[9] Lei, X. and Noda, N.A. (2002). "Analyses of dynamic response of vehicle and track coupling system with random irregularity of track vertical profile". *Journal of Sound and Vibration,* 258, 147-165.

[10] Lu, F., Kennedy, D., Williams, F.W. and Lin, J.H. (2008). "Symplectic analysis of vertical random vibration for coupled vehicle- track systems". *Journal of Sound and Vibration*, 317, 236-249.

[11] Nielsen, J.C.O. (2008). "High-frequency vertical wheel-rail contact forces – Validation of a prediction model by field testing". *Wear,* 265, 1465-1471.

[12] Nielsen, J. and Igeland, A. (1995). "Vertical dynamic interaction between train and track influence of wheel and track imperfections". *Journal of Sound and Vibration,* 187, 825-839.

[13] Specification (technical standard), Technical Report, RFI, 2011.

[14] Sun, Y.Q. and Dhanasekar, M. (2002). "A dynamic model for the vertical interaction of the rail track and wagon system". *International Journal of Solids and Structures*, 39, 1337-1359.

[15] Vostroukhov, A. and Metrikine, A. (2003). "Periodically supported beam on a visco-elastic layer as a model for dynamic analysis of a high-speed railway track". *International Journal of Solids and Structures,* 40, 5723-5752.

[16] Wu, T.X., Thompson, D.J. (2005). "An investigation into rail corrugation due to micro-slip under multiple wheel/rail interactions. *Wear,* 258, 1115–1125.

[17] Zhai, W., Wang, K. and Lin, J. (2004). “Modelling and experiment of railway ballast vibrations”. *Journal of Sound and Vibration* , 270, 673-683.

[18] Zhai, W. and Cai, Z. (1997). “Dynamic interaction between a lumped mass vehicle and a discretely supported continuous rail track”. *Computers and Structures,* 63, 987-997.

[19] Zhang, J., Gao, Q., Tan, S.J. And Zhong W.X. (2012). “A precise integration method for solving coupled vehicle-track dynamics with nonlinear wheel-rail contac”. *Journal of Sound and Vibration* , 311, 4763-4773.